Four component regular relativistic Hamiltonians and the perturbational treatment of Dirac's equation.

Sadlej, A.J.; Snijders, J.G.; van Lenthe, E.; Baerends, E.J.

published in
Journal of Chemical Physics
1995

DOI (link to publisher)
10.1063/1.468703

document version
Publisher's PDF, also known as Version of record

Vibrational spectra of water complexes with H_2, N_2, and CO

J. Sadlej
Department of Chemistry, University of Illinois at Chicago, Box 4348, Chicago, Illinois 60680 and Department of Chemistry, University of Warsaw, 02-093 Warsaw, Poland

B. Rowland and J. P. Devlin
Department of Chemistry, Oklahoma State University, Stillwater, Oklahoma 74078

V. Buch
Department of Physical Chemistry, The Hebrew University, Jerusalem, Israel and Department of Chemistry, University of Illinois at Chicago, Box 4348, Chicago, Illinois 60680

(Received 12 August 1994; accepted 16 December 1994)

Ab initio calculations are carried out on the $H_2O\cdots N_2$, $H_2O\cdots H_2$, and $H_2O\cdots CO$ complexes. Infrared spectra of the complexes are investigated, with an emphasis on the effect of weak bonding on the frequencies and the infrared intensities of the monomers. Connections are explored between the computational results and the experimentally measured infrared spectra of ice surfaces covered by H_2, N_2, and CO adsorbate. Additional issues addressed include the influence of the counterpoise correction on the equilibrium geometry of the complexes, and the analysis of the different contributions (exchange, dispersion, electrostatic) to the weak bonding, and to the frequency shifts. © *1995 American Institute of Physics.*

I. INTRODUCTION

Clusters of H_2O with gaseous atoms and molecules received considerable attention in the past, both from experimentalists and from theorists (e.g., Refs. 1–33). The long term goal of the investigation of such clusters is to gain insights into interactions of small molecules with water in condensed phase systems, e.g., in solutions, or on icy surfaces. While solutions or surface/adsorbate systems are much more complex than the small clusters, the intermolecular interactions in these weakly bonded systems are largely pair additive, and one can gain considerable insight to these systems by studying pair interactions between the component molecules. In the present paper we investigate theoretically a series of three clusters—$H_2O\cdots H_2$, $H_2O\cdots N_2$, and $H_2O\cdots CO$. In particular, we investigate the effects of weak bonding on the infrared frequencies and the intensities of the monomers. Computational results on the frequency shifts and the intensity changes in the dimers are compared to experimental results for gaseous adsorbates (H_2, N_2, and CO) on icy surfaces.

Ab initio studies were shown to be a valuable tool for studying the nature of weak bonding.[33,34] Weak intermolecular interactions are hard to calculate very accurately, since they correspond to small differences between large quantities. While at present the accuracy of *ab initio* potentials is well below spectroscopic, the qualitative shapes of the calculated potentials are believed to be reliable. One should emphasize that *ab initio* calculations are the only means available to obtain the potentials from first principles, without any initial assumptions on their shape. *Ab initio* calculations have been used extensively (e.g., Refs. 25–27,31–33,40–43) to attain qualitative understanding of the shape of the anisotropic potential, via decomposition of the interaction energy into four fundamental components (electrostatic, exchange, dispersion, and polarization). The *ab initio* mapping and analysis of the interaction potential for the three clusters $H_2O\cdots H_2$, $H_2O\cdots N_2$, and $H_2O\cdots CO$ was already carried out by us in the past for rigid monomers.[31–33] Here the studies of these clusters are extended to include (a) optimization of cluster geometries with respect to all coordinates, (b) comparison between the physical origin of the interaction energies in the three clusters in optimized geometries, and (c) the dependence of the potential on monomer vibrational coordinates, and calculation of infrared frequencies and intensities. Past *ab initio* studies of the $H_2O\cdots N_2$ and $H_2O\cdots CO$ complexes by other authors can be found in Refs. 19–22.

In this study we shall examine the effect of weak bonding on monomer frequencies and intensities. It has been known for a long time that weak bonding induces frequency changes in vibrational spectra of molecules; in fact, such frequency changes have been used for years to probe local environments of molecules in matrices, solutions and clusters, and on surfaces (e.g., Ref. 44). However, basic understanding of interactions that cause the frequency shifts is quite limited. Typically, researchers in the field assume simple phenomenological models for dependence of the potential on monomer vibrational coordinates, and use them to calculate the shifts (e.g., Refs. 22 and 44). For example, the intermolecular potential may be modeled as a sum of functions of interatomic distances, and the shifts in monomer frequencies are assumed to be due to a distortion of the monomer by such interatomic terms. Alternatively, frequency shifts are assumed to be dominated by one or a few specific intermolecular interaction terms (e.g., by the induced dipole–permanent dipole interaction, or induced dipole–induced dipole interaction); the asymptotic long range formulas are then used for these interactions, and the vibrational dependence is introduced via the derivative of the polarizability or of the dipole with respect to the vibrational coordinate. While such phenomenological models often work for specific systems, first principle understanding of interactions causing the shifts is still scarce. Another frequently encoun-

 0021-9606/95/102(12)/4804/15/$6.00

tered but (usually) poorly understood effect of weak bonding is a change in the infrared intensity. In some systems intensity changes due to weak bonding are quite dramatic. A well-known example is the very significant increase in the infrared OH stretch intensity, accompanied by a very significant frequency shift, upon formation of a hydrogen bond between a pair of water molecules; this remarkable effect was discussed theoretically in the past in Refs. 45–46. Another example to be discussed in this paper is an increase in intensity of the OH stretch band upon formation of weak bonding with CO.

In this paper we employ *ab initio* calculations to obtain first principle information on the frequency and intensity shifts in the three clusters. The present calculations are exploratory and highly approximate, employing predominantly harmonic normal mode analysis at optimized configurations for these highly anharmonic cluster systems. Because of the errors inherent to the calculations (the frequency shifts are generally small!), we are interested mainly in frequency and intensity changes and trends rather than in the absolute values. Frequencies and intensities are explored for different intermolecular configurations of the clusters. The physical origin of the frequency shifts is analyzed using *ab initio* methods mentioned above.[39–43]

The calculations are used to interpret experimentally measured spectra of adsorbates on ice surfaces. This part of the investigation is a part of our ongoing research program to study weak bonding of gaseous adsorbates (such as H_2, N_2, and CO) to the ice surface.[47–53] The experimental information is derived predominantly from the infrared absorption bands of the adsorbate and of the dangling OH (or OD) bonds on the ice surface. The dangling bonds are bonds of the surface water molecules, in which the H atom (or the D atom) is not engaged in hydrogen bonding with another water molecule. The infrared peak due to the dangling bonds is close to the gaseous HDO value, and well removed from the bulk ice band of hydrogen bonded OH (or OD) stretch. We have shown in the past that the dangling OH (or OD) spectral features shift upon exposure to adsorbate in a highly specific manner, and thus serve as a useful probe of bonding of the adsorbate to the surface.[47–53] Complementary information is available from the adsorbate infrared and Raman bands. Thus, the CO adsorbate band is a doublet, indicating the presence of two types of adsorption sites on the ice surface. One of these sites was shown to be associated with CO attachment to the dangling OH (or OD) bonds.[53] In the present study we summarize the experimental information on frequency shifts of dangling OH and OD bands upon exposure to H_2, N_2, and CO adsorbate, and the shifts in adsorbate bands with respect to the gas phase. Moreover, new data are presented on the changes in the dangling bond infrared intensity upon gas adsorption. Connections are explored between these data and the *ab initio* calculations on the $H_2O\cdots H_2$, $H_2O\cdots N_2$, and $H_2O\cdots CO$ dimers. While quantitative agreement is not expected in comparison between experimental data on complex condensed phase systems and *ab initio* calculations on dimers, *ab initio* calculations reproduce quite well some qualitative trends observed on the surface, including redshift and intensity enhancement of the OH stretch absorption upon attachment of a molecule to OH, in the order $H_2<N_2<CO$. The CO frequency shift is shown to depend on the configuration of CO with respect to the water molecule, in qualitative accord with the experimental results.

In addition to the investigation of vibrational spectra, the *ab initio* part of this study addresses some computational issues. The Gaussian packages[55] that allow automatic geometry optimization by using gradient technique led to the practice of determining geometries of H-bonded systems by automated search for the global minimum of the total energy of the complex. This procedure ignores the presence of the basis set superposition error (BSSE).[54] Several authors have investigated in the past the influence of the BSSE on the structure of the hydrogen bonded complexes.[25,31,56–60] It was found that the change in equilibrium distances after applying the counterpoise correction can be quite large.[57] Erroneous behavior of the BSSE-uncorrected potential energy surface (PES) was observed for several complexes involving the water molecule[25,31,59] and SCO.[60] One of the aims of this work is to show how the BSSE influences the equilibrium structure of the investigated systems. Preliminary results are also presented on the effect of BSSE on vibrational frequencies.

In Sec. II, experimental results are given. In Sec. III the computational work is described. The study is summarized in Sec. IV.

II. EXPERIMENT

A. Technique

Infrared spectra have been observed for H_2, N_2, CO adsorbed within the micropores of amorphous ice and at the surface of cubic ice nanocrystals. Measurements have focused on the position and intensity of the stretch-mode bands of the dangling-OH (OD) groups, which are characteristic of the icy surfaces, and on the variations of the band parameters when the ice surfaces are covered with these molecular adsorbates. As in previous studies, the amorphous ice sample films were prepared at the rate of $\sim 0.1\ \mu$/min by condensation of H_2O or D_2O vapor beams in vacuum.[50] Sampling at submicron adsorbate-gas pressures in the temperature range of 12 to 30 K made use of an infrared transparent substrate attached to the cold stem of an Air Products CS-202 closed-cycle refrigerator. Samples of amorphous ice, under gas pressures ranging from 5–300 Torr at 80 K, were prepared on an inner window of a modification of the liquid–nitrogen-cooled double-walled infrared cluster cell described previously.[51]

The ice nanocrystals were prepared as micron-thick deposits using a technique recently described in some detail.[52] The nanocrystals, formed in the gas phase of a static cluster cell at temperatures in the 75–85 K range, were allowed to diffuse to the end windows of the cluster cell, where deposits composed of ''separate'' clusters were formed. Repetitive loading/pumping cycles, using $\sim 1\%$ gaseous mixtures of

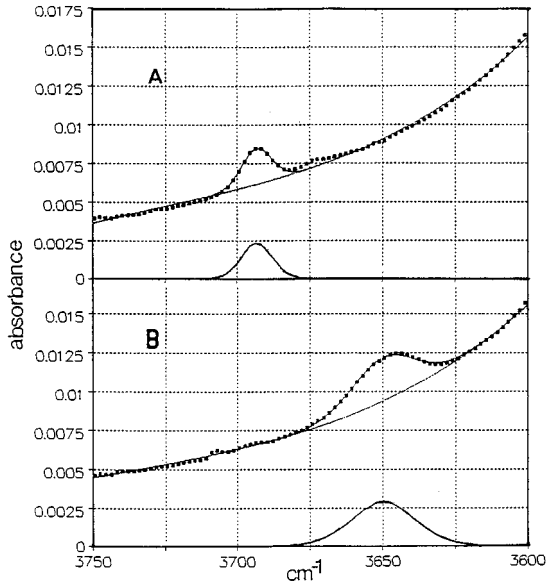

FIG. 1. Infrared bands of the dangling-OH-bond mode of ice at 80 K; (a) bare and (b) covered with CO under 20 Torr of CO(g). The curves ··· are for the original digitized spectra, while curves—represent the best mixed Gaussian–Lorentzian bands from the difference between the digitized spectra and the fitted backgrounds.

H_2O (D_2O) in N_2, produced ice deposits offering several advantages over direct sampling of the gas-phase nanocrystals. In the present study these advantages included (a) the use of long FT-IR scan times that yield the bands of the surface-localized modes, for the bare nanocrystals as well as with adsorbates, with the high signal-to-noise levels necessary for relative intensity measurements, (b) the ability to expose the crystals to adsorbates over a wide range of temperatures and pressures, and (c) the use of a single ice sample for several measurements, since a given volatile adsorbate may be sampled and removed in preparation for measurements using a second adsorbate.

FT-IR spectra were measured by coadding 256–1000 scans at nominal resolutions of either 2 or 4 cm^{-1} using either a Bio Rad FTS-20 or FTS-40 spectrometer. The weak bands (<0.01 peak absorbance) of the dangling-OH (OD) groups occur on the high-frequency wing of the intense bands of the bulk-ice stretching modes (~2.0 peak absorbance). As a result, it was necessary to fit the spectra to curved backgrounds in preparation for digital integration using the program PeakFit by Jandel Scientific. Repetitive relative band intensity measurements for a sample with a given adsorbate at a particular temperature and pressure, compared to band intensities of the bare ice, agreed to within 20%.

B. Experimental results

Typical spectra, showing the comparison of dangling-OH band intensities for the same ice *nanocrystals*, bare (3692 cm^{-1}) and covered with CO adsorbate molecules (3650 cm^{-1}) are presented in Fig. 1. It is clear from these spectra that the dangling-OH mode is downshifted and enhanced significantly by interaction with the CO molecules. Band positions and quantitative intensity-ratio values are given in Table I for the adsorbates H_2, N_2, and CO for amorphous and crystalline ice at low (15–30 K) and elevated (~80 K) temperatures. In general, these numbers indicate that both the band intensification and the downshift of the peak positions increase through the sequence of adsorbates H_2, N_2, and CO.

TABLE I. Band positions, frequency shifts, and the enhancement factors of the band intensity of the dangling OH (OD) vibrations of amorphous (I_a) and crystalline (I_c) ice relative to bare ice for the adsorbates H_2, N_2, and CO.

Sample	Position (cm^{-1})	Shift (cm^{-1})	Intensity ratio
H_2/I_a/12 K (D_2O)	2720	8	1.1
N_2/I_a/25 K (D_2O)	2709	19	2.5
N_2/I_a/85 K (D_2O)	2712	16	1.1
CO/I_a/30 K (D_2O)	2684	44	3.1
CO/I_a/30 K (H_2O)	3636	60	4.0
CO/I_a/85 K (D_2O)	2692	36	1.2
H_2/I_c/20 K (H_2O)	3683	9	1.1
N_2/I_c/20 K (H_2O)	3670	22	1.4
N_2/I_c/20 K (D_2O)	2708	18	1.5
N_2/I_c/85 K (H_2O)	3675	17	1.6
CO/I_c/76 K (D_2O)	2691	35	2.5
CO/I_c/85 K (H_2O)	3650	42	3.3

There is no evidence of a general pattern of differences of the enhancement factors for the amorphous versus the crystalline ice or of dangling-OH vs dangling-OD. (The main difference between the nanocrystal and amorphous ice surface is presumably the extent of surface roughness.) However, the magnitude of the band intensity ratio for N_2 and CO adsorbed on amorphous ice at ~25 K is significantly greater than at higher temperatures; or for N_2 on *crystalline* ice, regardless of temperature. This may reflect a reduced orientational mobility of the molecules adsorbed on the amorphous ice at low temperature, as one might anticipate a larger oscillating dipole for a configuration having the adsorbate molecule linear with the dangling-OH group.

The frequencies of the fundamental stretching modes of the diatomic adsorbate molecules can also be determined, for comparison with the computational values, either from infrared absorbance or Raman scattering. Infrared bands have been reported for H_2[50] and CO[53] adsorbed on amorphous ice, and are noted here along with new Raman and induced infrared results for N_2 on amorphous ice and infrared values for H_2 and CO on the surfaces of ice nanocrystals. The frequencies of the induced H_2 infrared bands vary with the time on the amorphous ice, but, after a few hours of relaxation at 12 K, have values near 4128 and 4140 cm^{-1} for ortho and para forms, respectively[50] [i.e., the $Q_1(1)$ and $Q_1(0)$ modes are shifted by 27 and 21 cm^{-1}, respectively, versus the gas phase values;[61] relaxation corresponds, presumably, to H_2 molecules diffusing to more stable sites on the surface]. By contrast, the bands for o–H_2 and p–H_2 adsorbed on ice nanocrystals are invariant with time at 4137 and 4145 cm^{-1}, indicating shifts of 18 and 16 cm^{-1} relative to $H_2(g)$.

Though the adsorbed H_2 molecules have stretch frequencies that vary somewhat with the nature of the surface sites of the amorphous ice, and the Raman peak frequencies tend to be blueshifted 2–4 cm^{-1} from the corresponding infrared

values, the stretch mode bands of $o-H_2$ and $p-H_2$ appear as single broadbands in each instance. On the other hand, the nature of the CO interaction at the different sites varies sufficiently to cause the appearance of two distinct bands, separated by 16 cm^{-1} [at 2152 and 2136 cm^{-1}, or shifted +9 and −7 cm^{-1} from CO(g) values[53]]. Similarly, a doublet with peaks at 2153 and 2137 cm^{-1} is observed for CO adsorbed on ice nanocrystals, and there is strong evidence that the higher-frequency band is caused by CO associated with the dangling OH bonds.[53] There is also some evidence that N_2 adsorbed on amorphous ice at 20 K produces two bands separated by ~4 cm^{-1}, as the infrared spectrum contains a dominant peak at 2330 cm^{-1} with a weaker shoulder near 2326 cm^{-1}. However, the Raman spectrum, which gives an intense stretch mode band and should be more reliable in this instance, consists of a single band centered at 2330 cm^{-1}. In either case, the shift from the $N_2(g)$ value of 2331 cm^{-1} is small.

III. *AB INITIO* CALCULATIONS

A. Computational details

Ab initio calculations were carried out using the GAUSSIAN92 computer code.[55] Correlation was included via the second-order perturbation theory (MP2 code). All calculations were made without the frozen-core approximation. High quality Gaussian basis set of the well-tempered type, containing three sets of polarization functions on all atoms was used to investigate the interactions.[21,22] This is $(14s8p/10s)-[7s6p/5s]$ basis set (WT),[62,63] augmented by the three d-symmetry polarization functions with the following exponents for O: 0.1, 0.3, 1.25, and C: 0.0705, 0.197, 0.659, and three p-symmetry functions for H: 0.1, 0.316, 1.0.[64] The exponents were optimized to best describe the interaction energy between the polar and polarizable systems. This basis set reproduces the SCF and MP2 energies of the monomers very well, and, moreover, it accurately treats the multipole moments and polarizabilities of the monomers. When applied to the intermolecular complexes this basis set is essentially free of the primary and secondary basis set superposition error at the SCF level.[64] The accurate reproduction of the molecular properties suggests that the components of the interaction energies are faithfully represented. Further extension of the basis set by adding the higher symmetry polarization functions should have a major effect only on dispersion energy, as the remaining terms (electrostatic, exchange, and induction) are, most likely, already saturated in this basis set.[64(a)]

The monomer properties calculated in the WT basis set are presented in Tables II and III. One of the concerns in calculations of weak interactions is a possible influence of the secondary BSSE, which appears as a result of changes in monomer properties due to the use of the dimer basis. Past studies[64] suggest that in the WT basis used in the present study the secondary BSSE should be negligible. We carried out several tests to verify this expectation for our systems. The dipole of H_2O was calculated in the dimer bases of the $H_2O\cdots CO$ and the $H_2O\cdots H_2$ global minima; the resulting values agreed within four digits with the dipole calculated in the monomer basis. For the CO dipole calculated in the monomer basis and in the $H_2O\cdots CO$ dimer basis, the agreement was even better. We also investigated the effect of the secondary BSSE on the dipole derivative of the $H_2O\cdots H_2$ complex with respect to the H_2 stretch, in the ohx configuration shown in Fig. 2(a) and discussed in detail in the following section. This configuration was selected, since the dipole derivative is small, so the BSSE effects could potentially be significant. The dipole derivative of the complex was calculated to be −0.002 99 a.u., while the BSSE in this quantity was only 0.000 04 a.u. (The BSSE is defined as in Ref. 64(c) as $[\mu'(H_2)+\mu'(H_2O)]_D-[\mu'(H_2)+\mu'(H_2O)]_M$,

TABLE II. The calculated monomer properties in the WT basis set (in a.u.) for the experimental geometry.[a]

E	H_2O	H_2	CO	N_2
E_{SCF}	−76.064 225	−1.133 223	−112.782 611	−108.985 474
$E(2)$	−76.337 313	−1.162 879	−113.174 144	−109.393 163
μ^{SCF}	−0.7810		−0.0987	
$\mu^{(2)}$	0.0507		0.2191	
μ_{tot}	−0.7303		0.1204	
μ_{exp}	0.724[82]		0.048[83]	
Θ_{xx}^{SCF}	1.917	0.6649	−1.7609	−0.927
$\Theta_{xx}^{(2)}$	0.047	−0.0299	−0.0656	−0.284
Θ_{yy}^{SCF}	−1.817			
$\Theta_{yy}^{(2)}$	−0.062			
$\Theta_{xx,tot}$	−1.964	0.635	−1.826	−1.211
$\Theta_{yy,tot}$	1.879			
$\Theta_{xx,exp}$	1.96[81(b)]	0.662[81(a)]	−1.85[81(a)]	−1.04[77(a)]
$\Theta_{yy,exp}$	−1.862			
α_{zz}^{SCF}	8.477	6.437	14.430	14.884
$\alpha_{zz}^{(2)}$	1.202	0.0004	1.216	−0.648
$\alpha_{zz,tot}$	9.679	6.437	15.646	14.236
α_{xx}^{SCF}	9.161	4.613	11.253	9.742
$\alpha_{xx}^{(2)}$	0.827	−0.066	0.688	0.309
$\alpha_{xx,tot}$	9.988	4.547	11.921	10.051
α_{yy}^{SCF}	7.896	4.613	11.253	9.742
$\alpha_{yy}^{(2)}$	1.648	−0.066	0.668	0.309
$\alpha_{zz,tot}$	9.544	4.547	11.921	10.051
$\alpha_{zz,exp}$	9.47[64]	6.939[84]	15.746[84]	15.094[84]
$\alpha_{xx,exp}$	9.68	4.820	12.169	10.370
$\alpha_{yy,exp}$	9.19	4.820	12.169	10.370

[a]Exp. geometry: r(OH)=0.9572 Å, α=104.52°, r(HH)=0.7408 Å, r(CO)=1.1283 Å, r(NN)=1.0943 Å.

TABLE III. The optimal geometry, the harmonic frequencies and the intensities for the monomers (MP2—full results, WT basis).[a,b]

E Geometry	H_2O	H_2	CO	N_2
r	0.9619	0.7387	1.1421	1.1216
α	104.22			
$E(2)$	−76.337 763	−1.162 883	−113.175 557	−109.331 702
ZPE	0.021 449	0.010 277	0.004 766	0.004 926
freq./int.				
ν_2	1630/70.9	4511/0.0	2092/36.05	2156/0.0
ν_1	3827/4.8			
ν_3	3957/70.8			

[a]The experimental values: H_2, r=0.7416, ω_e=4395 cm^{-1}; (Ref. 85) N_2, r=1.094 Å, ω_e=2360 cm^{-1}; CO, r=1.1281 Å, ω_e=2170 cm^{-1}; H_2O, r(OH)=0.9572, α=104.52, ω_1^0=3694; ω_2^0=1615, ω_3^0=3802 cm^{-1}. (Ref. 85)
[b]r in Å, E and ZPE in a.u., ν in cm^{-1}, and IR intensity in kM/mole.

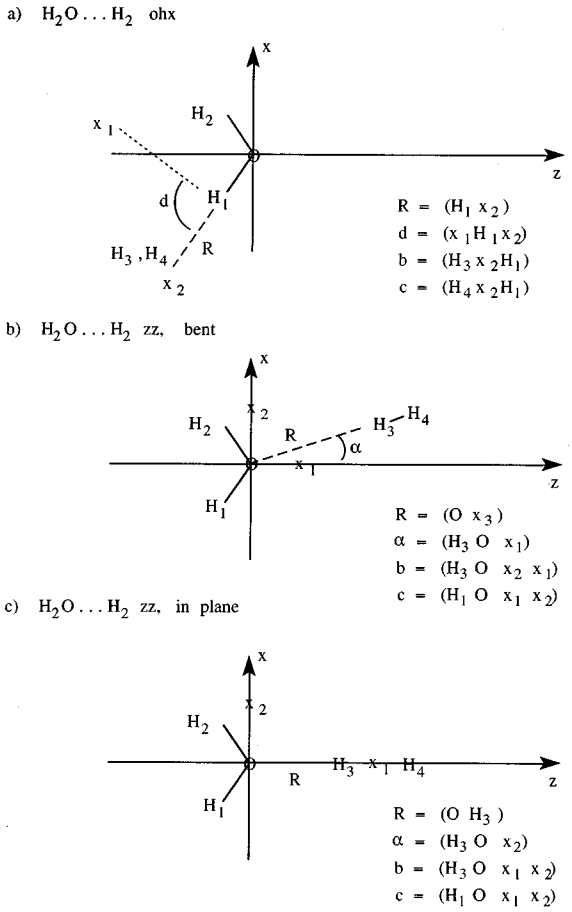

FIG. 2. The model structures of the $H_2O\cdots H_2$ complex. In (a) H_2 points into the page, and x_2 denotes location of the H_2 midpoint. In (b), H_2 points toward the O atom and lies approximately in the *yz* plane perpendicular to the water molecule. The (c) configuration is planar.

where the derivatives are with respect to the H_2 bond stretching, and the subscripts denote the dimer and the monomer basis sets, respectively.)

The analysis of the interaction energies was carried out using the Trurl package linked to GAUSSIAN88.[65] The vibrational calculations were performed using GAUSSIAN92 at the Cornell Theory Center.

B. The $H_2O\cdots H_2$ system

1. Search for equilibrium geometries; BSSE effects

The $H_2O\cdots H_2$ system was investigated by us in an earlier paper[31] in a different basis set. The objective there was mapping of the potential energy as a function of intermolecular configurations, the monomers were kept rigid and geometry optimization was not carried out. Two lowest-energy configurations located in that study are denoted *zz* and *ohx*, and are used here as starting points for geometry optimization [see Figs. 2(a) and 2(c)]. In the *zz* structure, H_2 approaches the O atom along the C_2 axis of H_2O [see Fig. 2(c)], while in the *ohx* structure H_2 forms a T-shaped structure with the OH bond of H_2O, with H_2 perpendicular to the water plane [see Fig. 2(a); H_2 center of mass location is at x_2, and the H_2 axis points into the page]. The geometry of these complexes was fully optimized at the MP2 level by using the gradient algorithm contained within the GAUSSIAN program. For the optimized structures, a complete set of vibrational frequencies and IR intensities was calculated.

TABLE IV. The MP2/WT geometries for two optimized structures of $H_2O\cdots H_2$.[a,b] The calculations without frozen core, 6*D* orbitals.

Parameters	$H_2O\cdots H_2$ (*ohx*)	$H_2O\cdots H_2$ (*zz*)
r(OH)	0.9619	0.9621
α(HOH)	104.3	104.2
r(HH)	0.7430	0.7433
R	2.3113	2.6319
α	79.0	23.9
b	89.0	83.5
c	89.1	172.5
E_{SCF}	−77.196 779	−77.197 002
$E(2)$	−77.500 211	−77.500 507
ZPE	0.033 281	0.034 340
CP-corr.		
ΔE_{SCF}	−54.522	−277.726
$\Delta E(2)$	−687.067	−819.981
CP-geom. corr.		
R	2.3669	2.7342
ΔE_{SCF}	−127.387	−385.238
$\Delta E(2)$	−692.812	−836.954

[a]See Fig. 2 for the definition of the different angles. Figure 2(a) is for *ohx* and Fig. 2(b) is for the *zz* structure.

[b]Bond lengths in Å, the angles in degrees, total SCF energy E_{SCF}, total MP2 energy $E(2)$, and ZPE energy in a.u.; CP-corr.-counterpoise (CP), corrected interaction energy for geometry obtained in gradient optimization, without CP geometry correction; ΔE_{SCF} and $\Delta E(2)$ in μH; CP-geom.corr.-CP corrected interaction energy for CP corrected geometry; ΔE_{SCF} and $\Delta E(2)$ in μH.

The parameters of the optimized structures and the harmonic frequencies at the two minima obtained in the WT basis are given in Tables IV and V. The different angles are defined in Fig. 2 [x_1 in Fig. 2(a) defines the direction perpendicular to the OH bond].

Gradient optimization of the *zz* structure resulted in the lower of the two minima. The optimized *zz* structure contains a linear O···H–H bond, with H–H in the plane almost perpendicular to the H_2O plane [see Fig. 2(b) and the last column in the Table IV]; the H_2 axis makes an angle of 23.9° with the C_2 axis of H_2O. It should be stressed that the rotation of the water molecule, such that the dihedral angle (H_1O,x_1x_2) changes from 172.5° to 180.0° and $b=(H_3O,x_1x_2)$ changes from 83.5° to 90.0° (i.e., H_2 is placed in the plane exactly perpendicular to the H_2O plane) increase the total MP2 energy by only 2 μH. In the optimized

TABLE V. The MP2/WT vibrational frequencies and IR intensities for the two optimized structures of $H_2O\cdots H_2$ (ν in cm^{-1}, I^{IR} in kM/mole).

	$H_2O\cdots H_2$ (*ohx*)		$H_2O\cdots H_2$ (*ohpr*[a])		$H_2O\cdots H_2$ (*zz*)	
Mode	ν	I	ν	I	ν	I
ν_1(OH sym. stretch)	3827	11.2	3823	11.6	3824	5.7
ν_2 (bend)	1631	60.5	1634	60.7	1632	69.3
ν_3 (OH asym. stretch)	3956	100.3	3952	92.6	3954	73.2
ν_4 (HH stretch)	4471	1.7	4474	1.8	4462	14.5

[a]A H-bonded configuration related to *ohx*, in which H_2 is rotated into the water plane, $R=2.4531$ Å, $b=76.47°$, $c=80.32°$ [see Fig. 2(a)].

ohx structure, the H_2 center is still in the water plane, however, it is removed 11° from the OH bond axis toward the water bisector; also, the H_2 axis is distorted slightly from the direction perpendicular to the H_2O plane.

As one can see from Table IV, the effect of hydrogen bond formation is to distort slightly the monomer subunits. The OH bond of water is stretched by 0.0002 Å in the *zz* complex. The HH bond is stretched by 0.0046 Å in *zz* and by 0.0043 Å in *ohx*. The energy-related aspects of the studied complexes are also reported in Table IV. It can be seen, that the electron-correlation contribution to the interaction energy calculated at the MP2 level is attractive and very important in determining the order and the magnitude of the stabilities.

The above results were obtained using the standard computer code, that does not take into account BSSE. BSSE correction to weak interactions is known to be important and often very substantial (even in ''good'' basis sets, see, e.g., Ref. 31). It is a common procedure in the literature to carry out optimization on the CP-uncorrected surface and to introduce the correction, only for the final energy of the optimized configuration. It has been noted, however, in the past that this procedure can lead to substantial errors in the equilibrium geometry.[25,31,56–60] For the $H_2O\cdots H_2$ cluster, the deficiencies of this procedure became very apparent in exploratory calculation carried out in the inferior 6-31G** basis. The optimized *zz* structure obtained in this basis is quite similar to that obtained in the WT basis, but the value of CP-corrected interaction energy $\Delta E(2)$ is *positive*!

To assess the effect of BSSE on the equilibrium geometry in the WT basis, we carried out a limited ''manual'' reoptimization of the *CP-corrected* equilibrium geometry and interaction energy $\Delta E(2)$.

We started by optimizing $R(O\cdots H)$ at the MP2 level using fixed subunit geometries taken from the full-geometry optimization in the WT basis set. Since calculations of Ref. 31 suggested that at the CP-corrected minimum the H_2 molecule should be in the water plane ($\alpha=0°$), we carried out the optimization both for the planar *zz* configuration with H_2 approaching along C_{2V} ($\alpha=0°$), and for the bent configuration obtained in optimization without BSSE correction ($\alpha=23°$). The CP-corrected MP2/WT calculations yield optimum $R(O\cdots H_3)=2.7319$ Å for the structure with $\alpha=23°$ and $R(O\cdots H_3)=2.7247$ Å for the structure with $\alpha=0°$ (C_{2V}). These values should be compared to the 2.6319 Å value obtained in optimization without BSSE for the bent *zz* structure. The bent structure ($\alpha=23°$) is slightly (19.6 μH=4.3 cm^{-1}) higher in energy than the structure with $\alpha=0°$. This is in agreement with calculations of Ref. 31 in a different basis, where it was shown that the potential well in the *zz* region is quite flat with respect to the bending of H_2 toward one of the lone pairs of H_2O, in the plane perpendicular to the H_2O plane.

We also carried out reoptimization of the $H_1\cdots x_2$ distance in the *ohx* structure [see Fig. 2(a)], for a configuration with $d=79°$, $b=89°$, $c=89°$ obtained from the BSSE uncorrected optimization. The minimum distance was found to be 2.3669 Å, to be compared with 2.3113 Å obtained without the BSSE correction. A reoptimized distance for a similar configuration with H_2 perpendicular to the H_2O plane ($d=b=c=90°$) was found to be 2.41 Å; the CP-corrected interaction energy was 19.2 μH=4.2 cm^{-1} lower than for the bent structure. The 11° deviation of the $OH\cdots x_2$ bond from linearity found in the CP-uncorrected optimization was found to remain valid for the CP-corrected optimization of a structure with $d=b=c=90°$ and the intermolecular distance of 2.41 Å.

(As noted above, the counterpoise correction has a much more dramatic effect on the results obtained with the poorer 6-31G** basis. Reoptimization of the intermolecular distances while using the CP correction changed the distances by 0.1–0.3 Å.)

The above calculations in the WT basis do not take into account the changes in the monomer geometries due to the CP correction. Of these the most important change is expected to be in the H_2 bond length. To evaluate this change, the calculations of the CP-corrected interaction energy were carried out as a function of r(HH). In the optimal configuration, the HH bond length was found to decrease with respect to the CP-uncorrected result by 0.0031 Å for bent *zz* ($\alpha=23°$) configuration, by 0.0039 Å for planar *zz*, and by 0.0032 Å for the *ohx* configuration. Reoptimization of r(HH) lowered the interaction energy by several μH.

We also checked the effect of the change of r(HH) on $R(O\cdots H)$, but this effect was found to be negligible, as well as the changes in the equilibrium geometry of the water molecule. Our ''best'' binding energies in the WT basis are -866.454 μH$=-190.2$ cm^{-1} for the *zz* configuration ($\alpha=0°$), and -700.051 μH$=-153.6$ cm^{-1} for the *ohx* structure. These values were obtained with BSSE correction for the planar *zz* configuration $\alpha=0°$, and for the *ohx* structure with H_2 perpendicular to the water plane, after reoptimization with BSSE correction with respect to the intermolecular distance and r(HH). In the case of *ohx*, we verified in addition that BSSE does not affect the optimal value of the angle between the OH bond and the intermolecular axis connecting the O atom with the center of H_2.

The optimized *zz* configuration with $\alpha=0°$ is thus more stable by 37 cm^{-1} than *ohx*. This result is in qualitative agreement with the results of Ref. 31, where the difference between the two forms in the $S(df)$ basis set was found to be 20 cm^{-1}. The higher stabilization of the *zz* form in the WT basis set is primarily due to improved description of the electrostatic, exchange, and deformation contributions, which seem to be saturated in this basis set.[64(a)]

As noted above, BSSE effects on the optimal geometry are much larger in the case of the inferior 6-31G** basis, than in the case of the WT basis used throughout this study. This result exemplifies the importance of a high quality basis set in gradient optimization studies of weakly bonded clusters.

2. Vibrational frequencies and intensities for $H_2O\cdots H_2$

Vibrational frequencies were calculated in the WT basis for the *zz* and *ohx* geometries obtained from gradient optimization. The standard GAUSSIAN code for the harmonic normal mode analysis was used. No attempt was made to include the BSSE corrections or the anharmonic corrections to the frequencies. As noted above, these frequency and inten-

sity calculations were designed predominantly to study trends and qualitative effects, rather than to calculate cluster spectra accurately.

The intramolecular vibrational spectra of the $H_2O\cdots H_2$ complex in the optimized *zz* and *ohx* configurations in the WT basis are given in Table V. In addition, we show results for another low-energy H-bonded configuration,[31] *ohpr*; this configuration was obtained by the rotation of H_2 in *ohx* into the water plane, followed by gradient optimization constrained to the water plane (in plane optimization yielded one imaginary intermolecular frequency). The two OH stretch frequencies are redshifted with respect to the monomer by 3 cm^{-1} in the *zz* structure, and by 4–5 cm^{-1} in *ohpr*; in *ohx* the change in the two frequencies is $\leqslant 1$ cm^{-1}. The change in the OH stretch intensities is much larger in the two H-bonded configurations than in *zz*; in *ohx* the ν_1 intensity is enhanced by factor 2.3, and ν_3 intensity—by factor 1.4, while in *zz* the intensities are close to the free molecule values. The H_2 stretch frequency is redshifted by 40 cm^{-1} in *ohx*, 37 cm^{-1} in *ohpr*, and 49 cm^{-1} in *zz*—this is a remarkably large shift. The (induced) infrared intensity of the H_2 stretch in the *zz* configuration is larger than in the two H-bonded configurations by factor ~8.5. We did not include in Table V the harmonic intermolecular frequencies for $H_2O\cdots H_2$, since their significance is doubtful. This is because of the very high anharmonicity and the weak intermolecular bonding in this complex.[29]

One may attempt to connect these results to experimental data.

Table I shows the effects of H_2 adsorbate on the dangling OH and OD bonds of ice. The measured frequency shifts (8–9 cm^{-1}) are larger than the ones calculated for H_2O bonded to a single H_2 molecule ($\leqslant 5$ cm^{-1}), indicating, perhaps, that the shift in the dangling OH band on the ice surface is some kind of collective effect of interaction of OH with a number of H_2 adsorbate molecules, rather than with a single one. This idea is also consistent with our simulations of H_2 adsorption on amorphous ice at 12 K (under conditions mimicking the experiment), which show that the surface is packed with H_2 molecules.[50(b)] Slight increase in the intensity of the dangling bond absorption upon exposure to H_2 is in qualitative accord with the computational results (see Table I).

Moroz and co-workers[66] reported a 4129 cm^{-1} infrared band in the Ar matrix, which they assigned to ortho H_2 in the $H_2\cdots H_2O$ dimer; this band is redshifted 26 cm^{-1} with respect to the gas phase and 9 cm^{-1} with respect to ortho H_2 isolated in Ar. Interestingly, they did not find a para H_2 band. Our Diffusion Monte Carlo studies of the dimer[29] indicated that due to zero-point motion effects para H_2 is bonded to the H atom of water (as in the *ohx* configuration, however, H_2 is orientationally delocalized by zero-point motion), while ortho H_2 can bond both to the H atom and to the O atom (as in *zz*). The experimental results thus appear qualitatively consistent with much larger induced infrared intensity obtained for the *zz* configuration than for *ohx* and *ohpr*.

As noted in Sec. II, both ortho H_2 and para H_2 Q_1 vibrational bands were observed spectroscopically in studies of H_2 adsorbate on ice. The adsorbate stretch bands are redshifted by 27–16 cm^{-1} with respect to the gas phase. These values are similar to the shift reported by Moroz *et al.*[66] for the ortho—$H_2\cdots H_2O$ dimer in Ar. Our calculated H_2 frequency shifts for the two minimum configurations in the isolated $H_2O\cdots H_2$ dimer are in the right direction (redshifts), but larger by about a factor of 2.

At this point one may ask whether the fact that the calculated H_2 redshift is much larger than in experiments has something to do with approximations used in the present calculation. To address this point (at least partially) we proceeded to remove some of the approximations; i.e., we calculated BSSE corrected H_2 frequencies for the BSSE corrected minima, and included the bond anharmonicity. This was done as follows. The BSSE corrected interaction energy was calculated for the two minimum energy configurations, while varying the H_2 bond length between 1 and 2 bohr (15 points were calculated in this interval). We added to the resulting interaction energy the energy of isolated H_2 as a function of bond length. The result, which represents the dependence of the cluster energy on the H_2 stretch was fitted to a Morse function; the rms of the fit was about 40 cm^{-1}, and the energy range of the fit was 0–10 000 cm^{-1} above the minimum. Standard Morse formulas were then used to obtain the H_2 frequency from the difference between the Morse ground state, and the first excited state. The result was compared to similarly calculated Morse frequency of isolated H_2. [The obvious question in this calculation is whether one should use for isolated H_2 the monomer basis, or the dimer basis. Fortunately, the H_2 frequencies obtained in the three basis sets are very similar—4305 cm^{-1} (monomer), 4304 cm^{-1} (*ohx* dimer basis), and 4306 cm^{-1} (*zz* dimer basis)]. The H_2 Morse frequencies in the *zz* and *ohx* configurations are 4280 and 4289 cm^{-1}, redshifted about 25 and 16 cm^{-1} with respect to the gas phase. These shifts are much closer to the experimental range of values given above.

The above exercise is not (of course) designed to provide the ultimate vibrational frequencies. An accurate calculation would require adjustment of the basis to obtain a better match with the gaseous H_2 frequency, and averaging over a broad range of intermolecular configurations characteristic of this complex.[29] This exercise demonstrates, however, numerically the (fairly well-known) fact that frequency shifts obtained from the normal mode analysis of minima are, at most, of qualitative significance, and that quantitative agreement with experiments, if obtained in such a calculation, is most probably due to a coincidental cancellation of errors.

C. $H_2O\cdots CO$ and $H_2O\cdots N_2$

1. Geometry optimization, effects of BSSE

In this part we report the structures, the energetics, and the frequencies for the dimers formed by H_2O with CO and with N_2. The potential energy surfaces of the complexes were investigated at the MP2/WT level. The in-plane intermolecular parameters employed here are defined in Fig. 3. These include the intermolecular distance R and the angles α and β corresponding to the rotations of the monomers with respect to the intermolecular axis. The *x* point in Fig. 3 is in the midpoint of the respective diatomics.

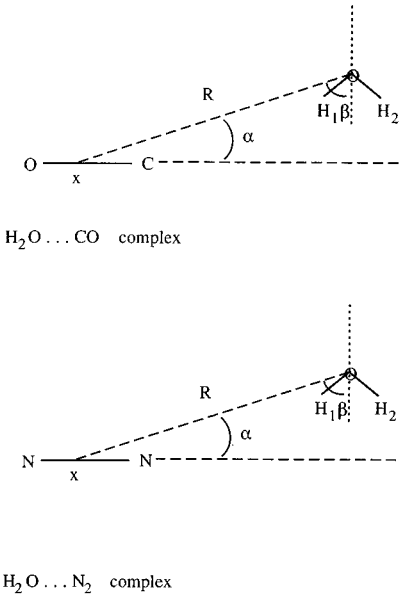

FIG. 3. The model structure of (a) $H_2O\cdots CO$; (b) $H_2O\cdots N_2$.

Global optimization yielded equilibrium structures in which the diatomic is bonded to a H atom of water in an approximately collinear configuration $OH\cdots CO$ or $OH\cdots NN$. This optimized geometry is in accord with microwave data,[1,2] *ab initio* mapping of the potential, which was carried out by us in the past in different basis sets,[32,33] and other *ab initio* studies of these clusters[19–22,67] (the latter studies were carried out without the BSSE correction). The parameters of the optimized structures are given in Tables VI and VII. For $H_2O\cdots CO$, we found an extra H-bonded minimum for the $OH\cdots OC$ configuration; in accord with previous studies bonding via O of CO was found to be significantly weaker than bonding via C.[20]

There is a discussion in the literature concerning a possibility of an extra minimum in the two complexes, in which the diatomic is bonded to the O atom of water, in a T-shaped configuration.[20–23] We did not find such a minimum in the WT basis; minimization starting from the T configuration ended at the H-bonded minimum. Still, we calculated an optimized planar T configuration in which the diatomic was constrained to be perpendicular to the intermolecular axis, and the C_{2V} axis of water was directed along the intermolecular axis (α=90; β=180°, see Fig. 3). This configuration was found to have one imaginary frequency in the case of $H_2O\cdots N_2$ and two in the case of $H_2O\cdots CO$. The energies of the O-bonded T-shaped configurations were found to be significantly higher than of the H-bonded configurations (-166 cm^{-1} in $H_2O\cdots N_2$ and -351 cm^{-1} in $H_2O\cdots CO$).

The arrangement of the heavy atoms in the global minimum H-bonded configurations is not fully collinear. The absolute minimum occurs when the axis of the complex $O\cdots x$ (see Fig. 3) is 11° off the NN axis in the $NN\cdots HOH$ complex, and 10° off the CO axis in $OC\cdots HOH$. Also, the hydrogen bonding is nonlinear. At equilibrium, the OH bond of water makes an angle of 14° with the $O\cdots X$ axis of the complex for $NN\cdots HOH$, and 11° for $OC\cdots HOH$. In the secondary high-energy $CO\cdots HOH$ minimum, there is a similar deviation from collinearity of 12° between CO and $O\cdots x$ and of 17° between the OH bond and the $O\cdots x$ axis.

The difference in the optimized bond length of the free and the bonded OH in water is less than 0.0001 Å.

The well depths calculated as the BSSE corrected difference in energy between the complex and the monomers are -2796.345 $\mu H=-614$ cm^{-1} and -1816.933 $\mu H=-399$ cm^{-1} for the $H_2O\cdots CO$ and $H_2O\cdots N_2$ complexes, respectively. In $H_2O\cdots N_2$, the N_2 bond length is very similar to the monomer value, while in $H_2O\cdots CO$, the CO bond length is shortened by 0.0015 Å for $OC\cdots HOH$, elongated by 0.0005 Å for $CO\cdots HOH$, and shortened by 0.0003 Å for the T-shaped conformer. The most significant changes in r(OH)

TABLE VI. The MP2/WT optimized geometrical parameters for two structures of $H_2O\cdots N_2$.[a]

Parameters	$H_2O\cdots N_2$, H bond	$H_2O\cdots N_2$, T shaped (C_{2V})
r(OH)	0.9629	0.9621
α(HOH)	104.4	104.2
r(NN)	1.1210	1.1206
R(O···X)	3.816	3.2734
α	11.1	90.0[b]
β	66.5	180.0
E_{SCF}	−185.043 576	−185.043 326
E(2)	−185.735 972	−185.734 871
ZPE	0.027 896	0.026 754
CP-corr.		
ΔE_{SCF}	−156.308	178.852
ΔE(2)	−1816.933	−1059.837
CP-geom. corr.		
R	3.858	3.2834
ΔE_{SCF}	−286.287	156.498
ΔE(2)	−1835.959	−1062.254

[a]For the notation and the units, see Table IV. For the definitions of the geometrical parameters, see Fig. 3.
[b]One frequency imaginary, frozen α=90.0°, β=180.0°.

TABLE VII. The MP2/WT optimized geometrical parameters for three structures of $H_2O\cdots CO$.[a]

Parameters	$OC\cdots H_2O$	$CO\cdots H_2O$	$H_2O\cdots CO$ (T)
r(OH)	0.9626	0.9619	0.9621
α(HOH)	104.52	104.4	104.2
r(CO)	1.1406	1.1426	1.1418
R(O···X)	3.8777	3.7908	3.2384
α	9.7	167.8	90.0[b]
β	63.5	68.8	180.0
E_{SCF}	−188.845 578	−188.845 691	−188.845 161
E(2)	−189.516 619	−189.515 002	−189.514 828
ZPE	0.027 955	0.027 447	0.026 653
CP-corr.			
ΔE_{SCF}	−517.456	−924.183	−368.081
ΔE(2)	−2796.345	−1072.721	−1196.802
CP-geom. corr.			
R(O···X)	3.9176	3.8910	3.2950
α	9.78	167.8	90.0
ΔE_{SCF}	−717.624	−1056.123	−448.265
ΔE(2)	−2807.774	−1113.584	−1203.884

[a]For the notation and the units, see Table IV. For the definitions of the geometrical parameters, see Fig. 3. O···X is defined as a distance from O to the midpoint of CO.
[b]Frozen α=90.0°, β=180.0°.

TABLE VIII. The MP2/WT vibrational frequencies and IR intensities for two structures of $H_2O\cdots N_2$ (ν in cm^{-1}, I^{IR} in kM/mole). Full calculation with 6*D* orbitals.

	$H_2O\cdots N_2$, H bond		$H_2O\cdots N_2$, T shaped	
Mode	ν	I	ν	I
ν_2(HOH bend)	1635	53.9	1630	71.6
ν_1(OH sym stretch)	3819	23.4	3824	5.1
ν_3(OH asym stretch)	3947	149.3	3954	72.3
ν_4(NN stretch)	2161	0.3	2163	0.0
ν_5	53	10.6	*i*	
ν_6	76	18.7	14	228.4
ν_7	92	0.1	33	0.0
ν_8	192	86.1	65	19.9
ν_9	266	65.3	61	0.0

were found in the minimum HOH···NN configuration (0.001 Å) and HOH···CO (0.0007 Å).

Similar to the $H_2O\cdots H_2$ complex, we made some effort to correct "manually" the optimized dimer geometries for BSSE. We started by optimizing the α angle (see Fig. 3) using fixed subunit geometries taken from full-geometry optimization in the WT basis sets. We found that the α angle optimization has a very small effect on the binding energy. Using quadratic interpolation we found that the value of α obtained in the BSSE uncorrected optimization is in error by no more than 2°. Examination of the variation of the BSSE corrected interaction as a function of R(O···C) and R(O···N) showed that the BSSE correction to the optimal intermolecular distance does not exceed 0.1 Å.

2. Frequencies and intensities

The calculated harmonic frequencies and intensities are presented in Tables VIII and IX. (No attempt was made to correct the frequencies for BSSE or for anharmonicity.) In the stable conformers of HOH···CO and HOH···NN, the OH stretch frequencies of H_2O decrease with respect to a monomer. The decrease is 15 and 18 cm^{-1} for the symmetric and antisymmetric stretch in HOH···CO, and 8 and 10 cm^{-1}, respectively, in HOH···NN. There is a significant increase in the stretch intensity—by factor 9.4 and 2.3 for the symmetric and antisymmetric stretch of HOH···CO, and by factor 4.9 and 2.1 for the symmetric and antisymmetric stretch of HOH···NN. The calculated HOH bending frequency is higher from the isolated H_2O frequency by 6 cm^{-1} in HOH···CO and by 5 cm^{-1} in HOH···NN. The bending intensity is lower than in the monomer; the decrease is by factor 1.5 in HOH···CO and by factor 1.3 in HOH···NN. This result appears related to an experimental observation that the bending intensity in ice is lower than in a water monomer.

TABLE IX. The MP2/WT vibrational frequencies and IR intensities for three structures of $H_2O\cdots CO$ (ν in cm^{-1}, I^{IR} in kM/mole). Full calculation with 6*D* orbitals.

	$OC\cdots H_2O$		$CO\cdots H_2O$		$H_2O\cdots CO$ (T)	
Mode	ν	I	ν	I	ν	I
ν_2(HOH bend)	1636	46.9	1631	57.1	1628	71.43
ν_1(OH sym stretch)	3812	44.9	3829	15.3	3824	5.43
ν_3(OH asym stretch)	3939	163.3	3957	127.7	3954	72.9
ν_4(CO stretch)	2104	31.5	2090	49.8	2095	33.7
ν_5	56	10.4	38	9.5	*i*	
ν_6	89	12.1	62	26.4	*i*	
ν_7	101	1.34	80	0.0	53	12.3
ν_8	219	81.9	146	89.8	62	1.2
ν_9	312	65.4	210	60.1	82	18.2

There is an interesting difference between the calculated frequency shift of the stretch vibration of N_2 and of the isoelectronic CO in the two dimers. In $H_2O\cdots N_2$, the N_2 stretch frequency in the H-bonded minimum configuration and the N_2 frequency in the O-bonded T configuration differ by only 2 cm^{-1} from each other, whereas in $H_2O\cdots CO$ the two frequencies differ by 9 cm^{-1}. The CO frequency is even lower in the H-bonded HOH···OC minimum; it is 5 cm^{-1} below the T-shaped configuration, and 14 cm^{-1} below the HOH···CO minimum. The frequency of CO in the H-bonded HOH···CO minimum configuration is +12 cm^{-1} above the gas phase, while the frequency shift of N_2 in $H_2O\cdots N_2$ minimum is only +5 cm^{-1}.

It is of interest to compare the calculated frequency shifts in the two dimers to the shifts in the ice/adsorbate systems. The calculated OH stretch shifts in the dimers can be compared to the experimental results for the shift in the dangling OH and OD bands due to bonding to CO and N_2 adsorbate (see the Introduction and Table I). The experimentally measured shifts to the red are in the range 16–22 cm^{-1} for the N_2 adsorbate on H_2O and D_2O, and 35–60 cm^{-1} for the CO adsorbate. The sign and the order of magnitude of the experimental shifts is similar to the calculation, however, the calculated shift is smaller by about a factor of 2–3. The discrepancy is not surprising, considering that in the dimer one diatomic molecule is connected to a single OH bond of water, while the shift occurs in frequencies of two OH stretch vibrations (symmetric and antisymmetric), which are delocalized over two bonds. On the other hand, we have shown in a recent study[52] that vibrational excitations of the dangling OH (or OD) bonds are localized on *single* dangling bonds; moreover, these bonds may interact with more than one diatomic adsorbate molecule. Also, collective effects are not included in the calculation; as discussed in Ref. 68, shifts in OH stretching frequency due to attachment of a gaseous molecule to a H atom can be enhanced by hydrogen bonding of a water molecule to another H_2O. (For example, the experimentally measured dangling-OD shift due to ethylene adsorbate[69] is 2.1 times larger than the OH stretch shift measured for the HOD–ethylene dimer.[70])

Thus, a larger shift in the OH stretch frequency is, in fact, expected in the adsorbate-surface system, as compared to the complex. We are encouraged by the fact that in pairs of experiments conducted under similar conditions, the frequency shift of the dangling OH or OD bonds due to the CO adsorbate is larger by about a factor of 2 than the shift due to N_2; which is similar to the calculated ratio of the OH stretch shifts in $H_2O\cdots CO$ and $H_2O\cdots N_2$ dimers. The increase in the intensity of the dangling bond infrared absorption by up to a factor of 2.5 upon adsorption of N_2, and up to a factor of 4.0 upon adsorption of CO is also qualitatively consistent with

the calculated increase in intensity of OH stretch bands in the $H_2O\cdots N_2$ and $H_2O\cdots CO$ dimers with respect to the monomer.

Our computational results are also fairly consistent with the measured spectra of the N_2 and CO adsorbate on ice (see the end of Sec. II). The CO adsorbate stretch band is a doublet.[53] The higher-frequency band was shown to be due to CO bonded to dangling OH (or OD) bonds; this band is shifted by $+9$ cm^{-1} with respect to CO(g), which compares quite favorably with the $+12$ cm^{-1} shift calculated for CO in the H-bonded configuration of $H_2O\cdots CO$. The lower-frequency band is shifted by -7 cm^{-1} with respect to the gas phase, and corresponds to CO attached to other binding sites on the ice, away from the dangling bonds. These sites may be in the vicinity of dangling O atoms on the surface (a dangling O atom is an O atom with a ''missing'' hydrogen bond); but most probably correspond to CO adsorbed in a surface indentation and interacting with several water molecules at a time.[50,53] While similar many body sites are not present in the dimer, we examined the difference in the CO frequency in three configurations: HOH$\cdots$CO, HOH$\cdots$OC, and a T-shaped configuration. The CO frequency shifts with respect to the gas phase in the three configurations are $+12$, -2, and $+3$ cm^{-1}, respectively. This result is consistent with the notion that the CO frequency shift is sensitive to the relative configuration of CO and the water molecule(s) with which it interacts. This is in contrast to N_2, in which the calculated shift in the dimer is much smaller and much less site sensitive than in the case of CO. Based on these computational results, one expects the N_2 adsorbate frequency to be less shifted with respect to the gas phase, and much less site sensitive than the CO adsorbate frequency. This expectation is born out by experiment; the measured N_2 stretch spectrum is either a single peak (Raman) or a peak with a weakly separated shoulder (infrared), and the shift with respect to the gas phase is not more than a few cm^{-1}. This result should be contrasted with the CO adsorbate spectrum, which consists of a well-separated doublet.

We are not aware of any measurements of vibrational spectra for the $H_2O\cdots N_2$ and $H_2O\cdots CO$ complexes in the gas phase. The spectra are available for these complexes in matrices,[10–12] however, the comparison with the present calculations is not straightforward, since the shifts in H_2O frequencies are strongly influenced by matrix effects. Thus, for example, in the case of $H_2O\cdots N_2$ in the Ar matrix,[12] the shift in the antisymmetric OH stretch/water bending/N_2 stretch is $-23.6/+4.9/-2$ cm^{-1} with respect to the gas phase, and $-2.5/+10.6/+1$ cm^{-1} with respect to H_2O and N_2 isolated in the Ar matrix; the calculated shifts at the minimum of the dimer with respect to gaseous H_2O and N_2 are $-10/+5/+5$ cm^{-1}.

The CO stretch frequency in the $H_2O\cdots CO$ complex was measured in the Ar matrix[11] (shift with respect to the gas phase: $+6$ cm^{-1}; shift with respect to CO isolated in the matrix: $+11$ cm^{-1}. A similar measurement in the O_2 matrix[10] indicated a shift of $+2$ cm^{-1} with respect to the gas phase, and 11 cm^{-1} with respect to the matrix. This value can be compared to the $+12$ cm^{-1} shift calculated by us with respect to the gas phase, and $+9$ cm^{-1} shift measured for CO adsorbate at the dangling OH (or OD) sites. The blueshift in the CO stretch frequency in the H-bonded dimer configuration seems to be generally characteristic of systems in which the carbon of CO is connected to a proton donor or to a positively charged ion. Similar increase in CO frequency was reported for matrix isolated complexes of CO with several proton donors, where CO functions as a proton acceptor,[10–12] for CO bonded to cations in zeolites,[71] for CO complexes with metal halide ligands in Ar matrices,[72] and for CO bonded to Na^+ on NaCl surfaces.[73]

TABLE X. The interaction energy and its components (in μH) for three configurations of the $H_2O\cdots H_2$ complex.

Energy	A[a]	B[b]	C[c]
ΔE_{SCF}	−378.389	−398.786	−127.387
$\Delta E(2)$	−837.179	−850.488	−692.812
$\Delta E^{(2)}$	−458.790	−451.702	−565.425
ΔE_{HL}	−77.001	−99.799	230.722
$\epsilon_{\mathrm{exch}}^{\mathrm{HL}}$	1072.732	1037.258	1098.638
$\epsilon_{\mathrm{es}}^{(10)}$	−1149.733	−1137.057	−867.916
$\Delta E_{\mathrm{def}}^{\mathrm{SCF}}$	−301.388	−298.987	−358.109
$\epsilon_{\mathrm{CHF}}^{(20)}$	−262.179	−263.092	−293.392
$\epsilon_{\mathrm{ind}}^{\mathrm{CHF}}$	−315.985	−316.563	−381.430
$\epsilon_{\mathrm{es},r}^{(12)}$	64.956	77.138	16.956
$\epsilon_{\mathrm{disp}}^{(20)}$	−767.538	−763.725	−704.449
$\Delta E_{\mathrm{exch}}^{(2)}$	243.792	234.885	122.068
SCFD[d]	−1145.927	−1162.511	−831.836

[a]A: $H_2O\cdots H_2$, *zz*, $R(O\cdots H_3)=2.7319$ Å, $\alpha=23.9$.
[b]B: $H_2O\cdots H_2$, *zz*, $R(O\cdots H_3)=2.7247$ Å, $\alpha=0.0$.
[c]C: $H_2O\cdots H_2$, *ohx*, $R(O\cdots X_2)=2.3663$ Å.
[d]SCFD means $\Delta E_{\mathrm{SCF}}+\epsilon_{\mathrm{disp}}^{(20)}$.

The assignment of the intermolecular harmonic frequencies given in Tables VIII and IX for the H-bonded minimum configuration is as follows. ν_5 and ν_6 are the librational modes of the diatomic; the lower-frequency vibration is in the complex plane, and the higher-frequency one—out of the plane. ν_7 is the intermolecular stretch vibration. ν_8 and ν_9 are the water librational modes. Again, the lower-frequency mode of this pair is in the complex plane, and the higher-frequency one—out of the plane. We are not aware of any published experimental data on the intermolecular frequencies of the three complexes of our interest. One can compare, however, our results to the experimental frequencies of the linear OC$\cdots$HF complex. For this complex, a frequency of 389.6 cm^{-1} was measured for the doubly degenerate HF librational mode of OC$\cdots$HF in the Ar matrix;[11] and frequencies of 125 cm^{-1} and 57 ± 12 cm^{-1} were estimated for the intermolecular stretch and for the degenerate low frequency CO libration from the analysis of the rotational spectra of the complex.[74,75] The calculated frequencies for $H_2O\cdots N_2$ and $H_2O\cdots CO$ given in Tables X and XI are reasonably consistent with these results. The ordering of the frequencies $OC\cdots HF > H_2O\cdots CO > H_2O\cdots N_2$ is the same as the ordering of the binding energies, as expected. The degeneracy of the librational modes is removed in our complexes, due to their nonlinearity.

Lower level calculations of the $H_2O\cdots N_2$ frequencies in the hydrogen bonded structure were carried out in the past in the smaller 4-31G and 6-311G** bases, employing RHF.[21]

TABLE XI. The interaction energy and its components (in μH) for the optimized configurations of $H_2O\cdots CO$ and $H_2O\cdots N_2$ complexes. Full calculation with $6D$ orbitals.

	$OC\cdots H_2O$	$CO\cdots H_2O$	$N_2\cdots H_2O$
ΔE_{SCF}	−571.456	−924.183	−156.834
$\Delta E(2)$	−2796.345	−1072.721	−1814.961
$\Delta E^{(2)}$	−2224.889	−148.538	−1658.127
ΔE_{HL}	737.511	357.576	622.473
ϵ_{exch}^{HL}	4501.857	1860.315	2756.713
$\epsilon_{es}^{(10)}$	−3764.347	−2217.891	−2134.239
ΔE_{def}^{SCF}	−1306.967	−566.607	−779.307
$\epsilon_{ind}^{(20)}$	−1316.638	−631.991	−823.743
ϵ_{ind}^{CHF}	−1647.445	−713.633	−955.414
$\epsilon_{es,r}^{(12)}$	−641.653	836.759	−451.841
$\epsilon_{disp}^{(20)}$	−2077.003	−1469.989	−1742.760
$\Delta E_{exch}^{(2)}$	493.767	484.692	536.474
SCFD	−2648.459	−2394.172	−1899.594

Another study of IR spectra was carried out on in Ref. 20 on the $H_2O\cdots N_2$ and $H_2O\cdots CO$ complexes at the MP2/6-31G** level. The blueshift in N_2/CO stretch and H_2O bending, and the increase in OH stretch intensity were obtained for the H-bonded minimum, and are in accord with the present study. The main difference with respect to our study is for OH stretch; in Ref. 21, OH stretch was calculated to be blueshifted, while in Ref. 20 much smaller [$(-5)\sim(+2)$ cm^{-1}] red- and blueshifts were obtained. This is in contrast to the present computational results and to the experimental results on the effect of N_2 adsorbate on the infrared bands of dangling OH. Parish *et al.*[22] obtained the intermolecular harmonic frequencies using the Molecular Mechanics for Clusters (MMC) potential; their frequencies are significantly lower than ours.

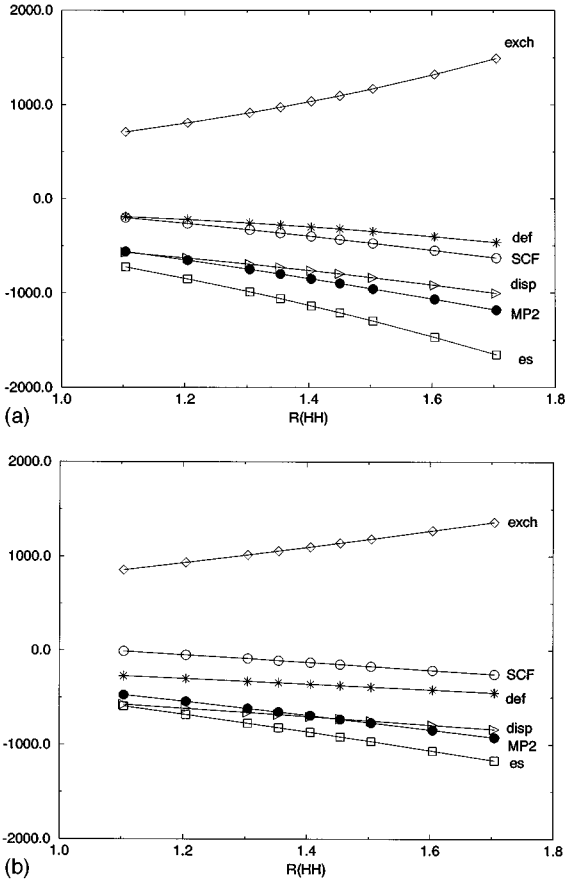

FIG. 4. Major stretch-dependent components of the interaction energy in the $H_2O\cdots H_2$ complex, as a function of R(HH) for (a) zz configuration, $\alpha=0°$; (b) ohx configuration. The following abbreviations have been used: SCF=ΔE_{SCF}, def=ΔE_{def}^{SCF}, es=$\epsilon_{es}^{(10)}$, disp=$\epsilon_{disp}^{(20)}$, MP2=$\Delta E(2)$, exch=ϵ_{exch}^{HL}. Energy in microhartree, distance in bohr.

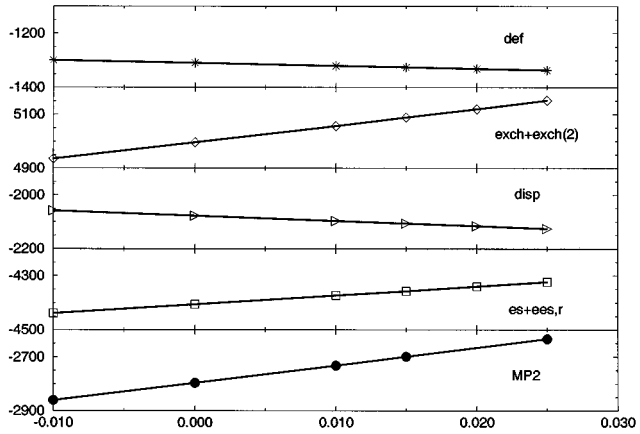

FIG. 5. Major stretch-dependent components of the interaction energy as a function of deviation of r(CO) from equilibrium, for the H-bonded configuration of the $H_2O\cdots CO$ complex. The following abbreviations have been used: def=ΔE_{def}^{SCF}, es=$\epsilon_{es}^{(10)}$, es,r = $\epsilon_{es,r}^{(12)}$, exch=ϵ_{exch}^{HL}, exch(2)=$\Delta E_{exch}^{(2)}$, MP2=$\Delta E(2)$. Energy in microhartree, distance in angstrom.

D. Analysis of the contributions to the potential surface

To better understand the differences in the stabilization between the three complexes and the origin of the vibrational shifts, the interaction energy components were analyzed in the WT basis set according to the procedure proposed and applied in Refs. 25–27,31–32,40–43,76. In this analysis the interaction energy is decomposed into components of different physical origins, such as electrostatic, dispersion, and exchange repulsion. The decomposition for the optimized configurations of the complexes is shown in Tables X and XI. The definitions of the different interaction components are presented below. More details on the partitioning used here can be found in Refs. 41 and 76. A similar analysis was carried out by us in the past for each of the three complexes[31–33] in different basis sets. The new feature here is the comparison between the optimized structures of the the three complexes obtained in the same high quality basis. An entirely new feature of the present analysis is the examination of the physical origins of the dependence of the intermolecular potential in the complexes on the diatomic stretch coordinates (see Figs. 4 and 5).

Our analysis focuses on ΔE_{SCF} and $\Delta E(2)$. The recently established scheme permits dissection of ΔE_{SCF} and of $\Delta E(2)$ into their components using perturbation theory of intermolecular forces. According to Ref. 41, ΔE_{SCF} consists of the following contributions:

$$\Delta E_{\mathrm{SCF}}=\Delta E_{\mathrm{HL}}+\Delta E_{\mathrm{def}}^{\mathrm{SCF}},$$

$$\Delta E_{\mathrm{HL}}=\epsilon_{\mathrm{es}}^{(10)}+\epsilon_{\mathrm{exch}}^{\mathrm{HL}},$$

where ΔE_{HL} is the Heitler–London contribution, and $\Delta E_{\mathrm{def}}^{\mathrm{SCF}}$ is the SCF-deformation contribution. The HL component is divided into electrostatic $\epsilon_{\mathrm{es}}^{(10)}$ and exchange terms. For large intersystem distances, $\Delta E_{\mathrm{def}}^{\mathrm{SCF}}$ may be interpreted as the induction energy. It is due to mutual polarization constrained by the Pauli principle. We also consider the second-order IMPPT approximation to $\Delta E_{\mathrm{def}}^{\mathrm{SCF}}$—mainly the uncoupled Hartree–Fock (UCHF) ϵ_{ind} and the coupled Hartree–Fock (CHF) $\epsilon_{\mathrm{ind}}^{\mathrm{CHF}}$, induction energies.

The total interaction energy through the second-order MPPT, $\Delta E(2)$, is represented as a sum of ΔE_{SCF} and $\Delta E^{(2)}$. The last one is partitioned as follows:[41,76]

$$\Delta E^{(2)}=\epsilon_{\mathrm{es},r}^{(12)}+\epsilon_{\mathrm{disp}}^{(20)}+\Delta E_{\mathrm{exch}}^{(2)}+\cdots\ ,$$

where $\epsilon_{\mathrm{es},r}^{(12)}$ denotes the second-order correlation correction to the electrostatic effect, $\epsilon_{\mathrm{disp}}^{(20)}$ is the dispersion interaction and $\Delta E_{\mathrm{exch}}^{(2)}$ is the second-order exchange-correlation term.

We first compare the energy components in the two optimized structures *zz* and *ohx* of $H_2O\cdots H_2$ (see Table X). The total interaction energy ΔE (MP2)$=\Delta E(2)$ is represented by the sum of ΔE_{SCF} and $\Delta E^{(2)}$, the second-order perturbation theory correction, which represents correlation effects. The correlation effects are very important in both structures, *ohx* and *zz*, but the ratio of $\Delta E(2)$ to ΔE_{SCF} is 5.4 for *ohx* and 2.2/2.1 for the *zz* structure, with $\alpha=23.9°/\alpha=0°$. Thus, the correlation effect is much more important for the *ohx* structure. The electrostatic term $\epsilon_{\mathrm{es}}^{(10)}$ represents the major attractive term and its contribution to ΔE_{SCF} is similar in both configurations. What makes the difference between the two configurations is the exchange repulsion term, which is much more important in the *ohx* configuration than in *zz*. This large repulsion cancels partially the dispersion and the deformation SCF attraction. The *zz* structure is favored by much smaller exchange repulsion than *ohx*. Both structures also benefit from a considerable electric polarization effect, as evidenced by substantial values of the $\Delta E_{\mathrm{def}}^{\mathrm{SCF}}$ deformation term. The electrostatic correlation term $\epsilon_{\mathrm{es},r}^{(12)}$ is repulsive and quite small. The second-order exchange effect amounts to 122.068 and 234.885 μH, i.e., to about 11% and 22% of the HL-exchange term in the *ohx* and *zz* structures, respectively. This is much less than for nonpolar systems.

We now carry out comparison between the electronic structures of the three complexes in their lowest-energy configurations: *zz* structure of $H_2O\cdots H_2$, and the two H-bonded structures of $H_2O\cdots N_2$ and $H_2O\cdots CO$ (see Tables X and XI). The three molecules H_2, N_2, and CO have substantial quadrupoles, CO has, in addition, a small dipole. The long-range electrostatic interaction with the water molecule is dominated by the interaction between the diatomic quadrupole and the water dipole. The quadrupole moment Θ of H_2 is positive. The Θ of N_2 is negative, since the electric moment of the σ lone pair along the NN axis is more significant than that of the π bonds about the axis. Carbon monoxide has a more negative quadrupole moment than the isoelectronic N_2, presumably due to the diffuse carbon lone pair. The relative

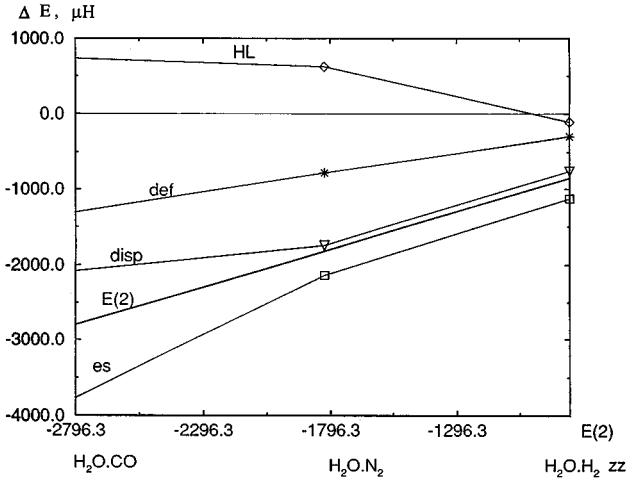

FIG. 6. The components of the interaction energy as a function of the total interaction energy for optimized geometries of the three systems: $H_2O\cdots H_2zz$, $H_2O\cdots N_2$, and $H_2O\cdots CO$.

order of the stabilities of the complexes is $H_2\cdots H_2O<N_2\cdots H_2O<OC\cdots H_2O$. The electrostatic components $\epsilon_{\mathrm{es}}^{(10)}$ represents the major attractive terms, followed by dispersion $\epsilon_{\mathrm{disp}}^{(20)}$ and the SCF-deformation components. As noted above, the exchange repulsion ($\epsilon_{\mathrm{exch}}^{\mathrm{HL}}$) is the smallest along the C_{2V} axis of water, and thus the HL term is negative in the $H_2O\cdots H_2$ *zz* complex, while it is quite large and positive in HOH$\cdots$NN, and even larger in HOH$\cdots$CO; in the latter two complexes the exchange repulsion is larger in size than the attractive electrostatic component $\epsilon_{\mathrm{es}}^{(10)}$. (The electrostatic and exchange terms are probably overestimated for the HOH$\cdots$CO complex, because of the overestimation of the CO dipole in the WT basis, see Table II.) The more negative quadrupole moment of CO and the presence of the dipole result in a stronger electrostatic interaction in HOH$\cdots$CO than in HOH$\cdots$NN. The SCF-deformation interaction constitutes 26% of $\epsilon_{\mathrm{es}}^{(10)}$ in $H_2\cdots H_2O$, 36% for $N_2\cdots H_2O$, and 34% for $H_2O\cdots CO$. In the second order the electron correlation gives rise to dispersion energy $\epsilon_{\mathrm{disp}}^{(20)}$, but also changes monomer permanent moments, thereby contributing to the second-order electrostatic correlation term $\epsilon_{\mathrm{es},r}^{(12)}$. This term is repulsive for $H_2O\cdots H_2$, but becomes significantly attractive for $H_2O\cdots N_2$, and even moreso for $H_2O\cdots CO$. The latter result is quite understandable in view of the fact that the correct sign of the CO dipole moment is obtained only at the MP2 level and that the quadrupole moment of N_2 increases in absolute value by $\sim$30% at the MP2 level (see Table II). However, in HOH$\cdots$NN, $\epsilon_{\mathrm{es},r}^{(12)}$ is cancelled by the second-order exchange effect $\Delta E_{\mathrm{exch}}^{(2)}$, which increases the total exchange repulsion, while partial cancellation occurs in HOH$\cdots$CO.

The main correlated attractive contribution is the dispersion interaction. On the relative scale of the total interaction energy, the dispersion energy is most attractive for $H_2O\cdots N_2$ (96% of the total energy), less so for $H_2O\cdots H_2$ (90%), and even less so for $H_2O\cdots CO$ (74%). To summarize these considerations, we displayed all the data in Fig. 6. The plots of this figure represent the contribution of the electrostatic, HL, SCF-deformation, dispersion, and electrostatic-correlation

terms as a function of the total interaction energy for the three systems. The electrostatic interaction and the SCF deformation dominate the left side of the figure, i.e., $H_2O\cdots CO$, while the relative contribution of dispersion is higher for $H_2O\cdots N_2$ and $H_2O\cdots H_2$.

One of the quantities of major interest in cluster studies is the influence of weak bonding on the intramolecular degrees of freedom. In Figs. 4(a) and 4(b) we show the dependence of the different interaction energy components on the H_2 stretch coordinate, around the estimated equilibrium distance, for the *zz* [Fig. 4(a)] and *ohx* [Fig. 4(b)] configurations of $H_2O\cdots H_2$. The interaction energy in the plots is defined as the difference between the energy of $H_2O\cdots H_2(R_{HH})$, and the sum of the energies of H_2O and $H_2(R_{HH})$ (all the energies were, of course, calculated in the dimer basis). Changes in R_{HH} cause monotonical changes in the different interaction components. The frequency of H_2 in the complex is determined by the equilibrium curvature of a sum of the intramolecular potential component and of the r(HH)-dependent terms in the intermolecular interaction. Since the latter terms do not display much curvature, their main effect appears to be the shift of the equilibrium R_{HH} distance to larger values, where the curvature of the intramolecular potential is smaller [also see Tables III, IV, and Refs. 13(b) and (c)]. Thus, the red frequency shift of H_2 in $H_2O\cdots H_2$ is due to the major bond stretching components of the interaction—electrostatic and dispersion, which in Fig. 4 have a negative slope. The negative slope can be related to the fact that both the quadrupole moment and the polarizability of H_2 increase, as the bond is stretched.[77] Another minor bond stretching component is $\Delta E_{\mathrm{def}}^{\mathrm{SCF}}$, which (as noted above) can be interpreted as the induction effect. The exchange repulsion, which has a positive slope, cancels partially the influence of the bond stretching interactions.

CO stretch dependence of the intermolecular potential components is shown in Fig. 5. In this case the bond compressing components (electrostatic and exchange) win over the bond stretching components (dispersion and deformation), resulting in a decrease in equilibrium bond length (see Tables 3 and 7), and in a concurrent increase in the CO stretch frequency. The positive slope of the electrostatic interaction in Fig. 5 is consistent with the fact that the dipole and the quadrupole of CO become less negative as the bond is stretched.[78] CO polarizability increases with bond stretching, resulting in the negative slope of the dispersion interaction in Fig. 5.

The present results are pertinent to commonly employed models for frequency shifts in weakly bonded systems, which assume that a *single* interaction component (say, induction or dispersion) is responsible for the observed shift. Our calculations suggest that generally one should expect *several* stretch-dependent components, which may cancel each other to a significant extent. Here one encounters a well-known difficulty in modeling of weakly bonded interactions—that these interactions are determined by the interplay between several terms of different signs and physical origins. *Ab initio* calculations emerge as an invaluable tool for elucidating the details of this interplay.

IV. SUMMARY

Ab initio calculations were carried in a well-tempered basis set (WT) on the MP2 level for the three clusters $H_2O\cdots H_2$, $H_2O\cdots N_2$, and $H_2O\cdots CO$. The calculations included optimization of geometries (including an investigation of BSSE effects on the optimized geometries and energies), analysis of the different contributions (electrostatic, exchange, and dispersion) to the intermolecular interactions near the minima, and calculation of the harmonic vibrational frequencies. In particular, we investigated changes in monomer frequencies and infrared intensities due to formation of the weak bonding. The frequency and intensity shifts were connected to experimental data on infrared spectra of ice surface/adsorbate systems, with H_2, N_2, and CO as adsorbates.

The minima were found to be dominated by electrostatic interactions between the anisotropic charge distributions of the monomers. H_2 has a quadrupole moment corresponding to extra negative charge in the middle, and extra positive charge at the edges. The quadrupole moment of N_2 and CO corresponds to an opposite charge distribution. CO has, in addition, a small dipole corresponding to extra negative charge on *C*. Two minima on the PES were found for the $H_2O\cdots H_2$ complex—one, in which H_2 approaches the O atom "edge on" on the C_{2V} axis (-190 cm^{-1}), and another in which H_2 is bonded via its middle to the H atom of water, and H_2 is perpendicular to the water plane (-154 cm^{-1}). For both $H_2O\cdots N_2$ and $H_2O\cdots CO$, a minimum was found for a configuration in which the diatomic is bonded "edge on" to the H atom of the OH bond in approximately collinear $OH\cdots NN$ and $OH\cdots CO$ arrangements (the deviation of OH and of the diatomic axis from collinearity is about 10°). These minimum configurations are in qualitative accord with past studies of these systems.[1–2,19–22,32–33] The minimum energies for $H_2O\cdots N_2$ and $H_2O\cdots CO$ were calculated to be -403 and -616 cm^{-1}. Minimization attempts starting from configurations in which N_2 or CO is bonded to the O atom of water via its middle (in a T-shaped configuration) ended in the H-bonded global minima. Constrained minimization in which the diatomic center of was was placed on the C_{2V} water axis, and the diatomic axis was perpendicular to C_{2V} resulted in O-bonded T-shaped configurations of significantly higher energies than the global minima (-166 cm^{-1} in $H_2O\cdots N_2$ and -351 cm^{-1} in $H_2O\cdots CO$).

Effects of the BSSE correction on the optimized geometries were investigated. In the case of $H_2O\cdots CO$ and $H_2O\cdots N_2$ hydrogen bonded complexes, the changes in equilibrium geometries due to the counterpoise correction were found to be quite small. Much larger sensitivity to the counterpoise correction was found in the $H_2O\cdots H_2$ complex, particularly in the O-bonded *zz* configuration. Gradient optimization yielded a C1 minimum in which H_2 is in the plane nearly perpendicular to H_2O, making a 23° angle with the water C_{2V} axis. After application of the BSSE correction, a planar structure in which H_2 lies on the C_{2V} axis was found to have lower energy. These calculations and also past studies[25,31,79] indicate that BSSE correction to the geometry is particularly important when an electrophilic species approaches the lone pair of oxygen.

Calculations of vibrational frequencies were carried out predominantly in the harmonic approximation, without BSSE correction, for the gradient-optimized structures. The results were compared to the experimentally measured vibrational spectra of the ice surface/adsorbate systems, with H_2, N_2, and CO adsorbates.[47–53] While one cannot expect quantitative agreement between calculated spectra of dimers and experimental spectra of many body adsorbate/surface systems, the calculations reproduced qualitatively a considerable number of experimentally observed effects, including (a) the redshift in H_2 frequency upon formation of a weak bond to water molecules (b) the blueshift in CO frequency upon formation of the weak OH···CO bond, and (c) the small effect of bonding to water on the N_2 frequency. The redshift in the H_2 frequency was shown to be due primarily to bond stretching by the electrostatic and dispersion components of the intermolecular interaction. The blueshift in CO frequency is a combined effect of the electrostatic interaction and the repulsive exchange component of the interaction, both of which increase when the CO bond is stretched.

The OH stretch frequencies in the dimers were found to be redshifted by the weak bonding with respect to gaseous water, in the order $H_2<N_2<CO$; the infrared stretch intensity was found to increase in the same order. These results are qualitatively consistent with the observed effect of H_2, N_2 and CO adsorbate on on the infrared band of the dangling OH and OD bonds on the ice surface. [The dangling bonds are bonds of water molecules in which H (or D) is not involved in hydrogen bonding to a neighboring water molecule[47–53]].

During the last ten years, numerous theoretical and computational studies were published on the nature of weak bonding in cluster systems. Theoretical investigations of the effects of weak bonding on monomer frequencies and intensities have been much more scarce; there are very few cluster systems for which such effects have been well understood (e.g., Refs. 45, 46, and 80). We are encouraged by the fact that the the present *ab initio* calculations appear to yield sensible qualitative results for frequency and the intensity changes in the dimers of water with three different gaseous molecules. On the other hand, our calculations confirm the well-known fact, that frequency shifts in molecular clusters obtained by an *ab initio* gradient minimization followed by normal mode analysis are (at most) of qualitative significance. We are currently carrying out detailed *ab initio* mapping of the dependence of the potentials for the $H_2O\cdots H_2$ and $H_2O\cdots CO$ clusters on monomer vibrational coordinates, including the counterpoise corrections. The potentials will be used in more accurate calculations of anharmonic vibrational spectra of the clusters, and of the adsorbate/ice systems.

Comment: After writing this paper, we became aware of a very recent *ab initio* calculation[86] on the structure and the vibrational frequencies of $H_2O\cdots CO$. The frequencies were calculated for the HOH···CO and the HOH...OC configurations in a smaller 6-31+$G(d)$ basis; the results are qualitatively similar to the ones given in the present paper. The intensities and the geometry parameters were not reported.

ACKNOWLEDGMENTS

We are grateful to Dr. S. M. Cybulski for the TRURL program and Dr. M. M. Szczęśniak and Dr. G. Chałasiński for commenting on the manuscript and for discussion. J.S. acknowledges the support of Grant No. BW-1219/20/94. The support of the National Science Foundation (NSF) Grant No. CHE-9022055 and of the BSF Grant No. 92-00180/1 is acknowledged by V.B. J.P.D. gratefully acknowledges NSF Grant No. CHE-902377. We thank the Cornell Theory Center for the allotment of the computer time.

[1] H. O. Leung, M. D. Marshall, R. D. Suenram, and F. J. Lovas, J. Chem. Phys. **90**, 700 (1989).
[2] D. Yaron, K. I. Peterson, D. Zolandz, W. Klemperer, F. J. Lovas, and R. D. Suenram, J. Chem. Phys. **92**, 7095 (1990); R. E. Bumgarner, S. Suzuki, P. A. Stockman, P. G. Green, and G. A. Blake, Chem. Phys. Lett. **176**, 123 (1991).
[3] G. Cazzoli, P. G. Favero, D. G. Lister, A. C. Legon, D. J. Millen, and Z. Kisiel, Chem. Phys. Lett. **117**, 543 (1985).
[4] A. C. Legon and L. C. Willoughby, Chem. Phys. Lett. **95**, 449 (1983).
[5] A. J. Fillery-Travis, A. C. Legon, and L. C. Willoughby, Chem. Phys. Lett. **98**, 369 (1983).
[6] K. I. Peterson and W. Klemperer, J. Chem. Phys. **80**, 2439 (1984); **81**, 3842 (1984); **85**, 725 (1986).
[7] F. J. Lovas, R. D. Suenram, G. T. Frazer, C. W. Gillies, and J. Zozom, J. Chem. Phys. **88**, 722 (1987).
[8] L. H. Coudert, F. J. Lovas, R. D. Suenram, and J. T. Hougen, J. Chem. Phys. **88**, 722 (1987).
[9] J. A. Odutola and T. R. Dyke, J. Chem. Phys. **72**, 5062 (1980).
[10] T. Tso and E. K. C. Lee, J. Phys. Chem. **89**, 1618 (1985).
[11] L. Andrews, R. T. Ailinghaus, and G. L. Johnson, J. Chem. Phys. **78**, 6347 (1983).
[12] L. Andrews and S. R. Davis, J. Chem. Phys. **83**, 4983 (1985).
[13] (a) R. E. Miller, D. F. Coker, and R. O. Watts, J. Chem. Phys. **82**, 3554 (1985); (b) J. R. Reimers and R. O. Watts, Chem. Phys. Lett. **94**, 222 (1983); (c) J. R. Reimers and R. O. Watts, Chem. Phys. **85**, 83 (1984).
[14] P. A. Block, M. D. Marshall, L. G. Pederson, and R. E. Miller, J. Chem. Phys. **96**, 7321 (1993).
[15] D. W. Steyert, M. J. Elrod, and R. J. Saykally, J. Chem. Phys. **99**, 7431 (1993).
[16] R. C. Cohen and R. J. Saykally, J. Chem. Phys. **95**, 7891 (1991); **98**, 6007 (1993).
[17] L. Dore, R. C. Cohen, C. A. Schmuttenmaer, M. J. Elrod, J. G. Loeser, and R. G. Saykally, J. Chem. Phys. **100**, 863 (1994).
[18] P. Herbine and T. R. Dyke, J. Chem. Phys. **83**, 3768 (1985).
[19] (a) L. A. Curtiss and C. L. Eisengruber, J. Chem. Phys. **80**, 2022 (1984). (b) A. E. Reed, F. Weinhold, L. A. Curtiss, and D. J. Pochatko, *ibid*. **84**, 5687 (1986).
[20] T. D. Mokomela, I. Recken, G. A. Yeo, and T. A. Ford, J. Mol. Struct. **273**, 33 (1992).
[21] D. B. Kitchen, T. P. Ruane, and L. C. Allen, Chem. Phys. Lett. **141**, 525 (1987).
[22] C. A. Parish, J. D. Augspurger, and C. E. Dykstra, J. Phys. Chem. **96**, 2069 (1992).
[23] K. A. Franken and C. E. Dykstra, Chem. Phys. Lett. **220**, 161 (1994).
[24] C. Bissonnette and D. C. Clary, J. Chem. Phys. **97**, 8111 (1992).
[25] M. M. Szczęśniak, G. Chałasiński, S. M. Cybulski, and P. Cieplak, J. Chem. Phys. **98**, 3078 (1993).
[26] M. M. Szczęśniak, G. Chałasiński, and S. M. Cybulski, J. Chem. Phys. **96**, 463 (1992).
[27] G. Chałasiński, M. M. Szczęśniak, P. Cieplak, and S. Scheiner, J. Chem. Phys. **94**, 2873 (1991).
[28] M. A. Suhm and R. O. Watts, Phys. Rep. **204**, 293 (1991).
[29] V. Buch, J. Chem. Phys. **97**, 726 (1992).
[30] Q. Zhang, N. Sabelli, and V. Buch, J. Chem. Phys. **95**, 1080 (1991).
[31] Q. Zhang, L. Chenyang, Y. Ma, F. Fish, M. M. Szczęśniak, and V. Buch, J. Chem. Phys. **96**, 6033 (1992).
[32] P. Sandler, J. oh Jung, M. M. Szczęśniak, and V. Buch, J. Chem. Phys. (in press).
[33] J. Sadlej and V. Buch, J. Chem. Phys. **100**, 4272 (1994).
[34] *Structure and Dynamics of Weakly Bound Molecular Complexes*, edited by

A. Weber, NATO ASI Series C (Reidel, Dordrecht, 1987), Vol. 212.
[35] *Dynamics of Polyatomic van der Waals Complexes*, edited by N. Halberstadt and K. C. Janda, NATO ASI Series B (Plenum, New York, 1990), Vol. 227.
[36] *Intermolecular Complexes. The Role of van der Waals Systems in Physical Chemistry and in the Biodysciplines*, edited by P. Hobza and R. Zahradnik (Academia, Prague, 1988).
[37] A. D. Buckingham, P. W. Fowler, and J. M. Hutson, Chem. Rev. **88**, 963 (1988).
[38] P. Hobza and R. Zahradnik, Chem. Rev. **88**, 871 (1988).
[39] G. Chałasiński and M. Gutowski, Chem. Rev. **88**, 943 (1988).
[40] G. Chałasiński and M. M. Szczęśniak, Chem. Rev. (in press).
[41] G. Chałasiński and M. M. Szczęśniak, Mol. Phys. **63**, 205 (1988).
[42] G. Chałasiński, M. M. Szczęśniak, and B. Kukawska-Tarnawska, J. Chem. Phys. **94**, 6677 (1991).
[43] H. L. Williams, K. Szalewicz, B. Jeziorski, R. Moszynski, and S. Rybak, Chem. Phys. **98**, 1279 (1993).
[44] *Vibrational Spectra of Trapped Species*, edited by H. E. Hallam (Wiley, New York, 1973); theoretical analysis of the shifts is given in the chapter by A. J. Barnes.
[45] J. G. C. M. van Duijneveldt-van de Rejdt, F. B. van Duijneveldt, J. A. Kanters, and D. R. Williams, J. Mol. Struct. **109**, 351 (1984); J. G. C. M. van Duijneveldt-van de Rejdt and F. B. van Duijneveldt, Chem. Phys. **175**, 271 (1993); J. Comput. Chem. **13**, 399 (1992).
[46] B. A. Zilles and W. B. Person, J. Chem. Phys. **79**, 65 (1983).
[47] J. P. Devlin, in *Physics and Chemistry of Ice*, edited by N. Maeno, Hokkaido University, Sapporo, 1992.
[48] (a) B. Rowland and J. P. Devlin, J. Chem. Phys. **94**, 812 (1991); (b) V. Buch and J. P. Devlin, J. Chem. Phys. **94**, 4091 (1991).
[49] B. Rowland, M. Fisher, and J. P. Devlin, J. Chem. Phys. **95**, 1378 (1991); J. Phys. Chem. **97**, 2485 (1993).
[50] (a) H. G. Hixson, M. J. Wojcik, M. S. Devlin, J. P. Devlin, and V. Buch, J. Chem. Phys. **97**, 726 (1992); (b) V. Buch and J. P. Devlin, *ibid*. **98**, 4195 (1993).
[51] F. Fuoad and J. P. Devlin, J. Phys. Chem. **93**, 7292 (1989).
[52] (a) J. P. Devlin, S. C. Silva, B. Rowland, and V. Buch, in *Hydrogen Bond Networks*, edited by M. C. Bellissent-Funel and J. C. Dore (Kluwer, Amsterdam, 1994); (b) B. Rowland, N. S. Kadagathur, J. P. Devlin, V. Buch, T. Feldmann, and M. J. Wojcik, submitted to J. Chem. Phys.
[53] J. P. Devlin, J. Phys. Chem. **96**, 6185 (1992).
[54] S. F. Boys and F. Bernardi, Mol. Phys. **19**, 553 (1970).
[55] GAUSSIAN92, M. J. Frisch, G. W. Trucks, M. Head-Gordon, P. M. Gill, H. W. Wong, J. B. Foresman, H. B. Schlegel, M. A. Robb, E. S. Replogle, R. Gomperts, R. L. Andres, B. G. Johnson, K. Raghavachari, J. S. Binkley, C. Gonzales, D. J. Defrees, D. J. Fox, J. Baker, R. L. Martin, J. J. P. Stewart, and J. A. Pople (Gaussian Inc., Pittsburgh, PA, 1992).
[56] Y. Bouteiller., Chem. Phys. Lett. **198**, 491 (1992); Y. Bouteiller and H. Behrouz, J. Chem. Phys. **96**, 6033 (1992).
[57] R. Eggenberger, S. Gerber, H. Huber, and D. Searles, Chem. Phys. Lett. **183**, 223 (1991).
[58] G. Algona, C. Ghio, R. Cammi, and J. Tomasi, Int. J. Quantum Chem. **32**, 207 (1987).
[59] J. G. C. M. van Duijneveldt-van de Rejdt and F. B. van Duijneveldt, J. Chem. Phys. **97**, 5019 (1992); J. Comput. Chem. **13**, 399 (1992).
[60] J. Sadlej and D. W. Edwards, Int. J. Quantum Chem. **46**, 623 (1993).
[61] B. F. Stoicheff, Can. J. Phys. **35**, 730 (1957).
[62] S. Huzinaga and M. Klobukowski, J. Mol. Struct. **167**, 1 (1988).
[63] S. Huzinaga, M. Klobukowski, and H. Tatewaki, Can. J. Chem. **63**, 1812 (1985).
[64] (a) M. M. Szczęśniak, S. Scheiner., Coll. Czech. Chem. Commun. **53**, 2214 (1988); (b) G. Karstrom and A. J. Sadlej, Theor. Chim. Acta **61**, 1 (1982); (c) M. M. Szczęśniak and S. Scheiner, Chem. Phys. Lett. **131**, 230 (1986).
[65] S. M. Cybulski, TRURL package, Carbondale, 1989.
[66] A. Moroz, R. L. Sweany, and S. L. Whittenburg, J. Phys. Chem. **94**, 1352 (1990).
[67] K. I. Peterson, G. T. Frase, D. D. Nelson, Jr., and W. Klemperer, in *Comparison of Ab Initio Quantum Chemistry with Experiment for Small Molecules*, edited by R. J. Bartlett and D. Reidel, 1985, p. 217.
[68] G. Maes and J. Smets, J. Phys. Chem. **97**, 1818 (1993).
[69] S. C. Silva and J. P. Devlin, J. Phys. Chem. (in press).
[70] A. Engdahl and B. Nelander, Chem. Phys. Lett. **113**, 49 (1992).
[71] C. L. Angell and P. C. Schaffer, J. Phys. Chem. **70**, 1413 (1966).
[72] R. H. Hauge, S. E. Gransden, and J. L. Margrave, J. Chem. Soc. Dalton Trans. 745 (1979).
[73] G. E. Ewing, Int. Rev. Phys. Chem. **10**, 391 (1991).
[74] A. C. Legon, P. D. Soper, and W. H. Flygare, J. Chem. Phys. **74**, 4944 (1981).
[75] E. K. Kyro, P. Shoja-Chaghervand, K. McMillan, M. Eliades, D. Danzeiser, and J. W. Bevan, J. Chem. Phys. **79**, 78 (1983).
[76] R. Moszynski, S. Rybak, S. M. Cybulski, and G. Chałasiński, Chem. Phys. Lett. **166**, 609 (1990); S. M. Cybulski, G. Chałasiński, and R. Moszynski, J. Chem. Phys. **92**, 4357 (1990); S. M. Cybulski, *ibid*., **97**, 7545 (1992); G. Chałasiński, M. M. Szczęśniak, and S. M. Cybulski, *ibid*., **92**, 2481 (1990); M. M. Szczęśniak, G. Chałasiński, and S. M. Cybulski, *ibid*. **93**, 4243 (1990); G. Chałasiński, M. M. Szczęśniak, S. M. Cybulski, S. Scheiner, *ibid*., **91**, 7809 (1989).
[77] J. D. Poll and L. Wolniewicz, J. Chem. Phys. **68**, 3053 (1978); W. Kolos, and L. Wolniewicz, J. Chem. Phys. **46**, 1426 (1967).
[78] G. H. F. Diercksen and A. J. Sadlej, Chem. Phys. **96**, 17,43 (1985); V. Kello, J. Noga, and A. J. Sadlej, Chem. Phys. Lett. **152**, 387 (1988).
[79] F. Haase, J. Sauer, and V. Kello, Chem. Phys. Lett. **174**, 19 (1990).
[80] See, e.g., D. C. Clary, J. Chem. Phys. **96**, 90 (1992); J. M. Hutson, J. Phys. Chem. **96**, 4237 (1992).
[81] (a) D. E. Stogryn and A. P. Stogryn, Mol. Phys. **11**, 371 (1966); (b) J. Verhoeven and A. Dynamus, J. Chem. Phys. **52**, 3222 (1970).
[82] G. H. F. Diercksen, B. O. Roos, and A. J. Sadlej, Int. J. Quantum Chem. Q. Sym. **17**, 265 (1983).
[83] J. S. Muenter, J. Mol. Spectrosc. **55**, 490 (1975).
[84] N. J. Bridge and A. D. Buckingham, Proc. R. Soc. London Ser. A **295**, 334 (1966).
[85] (a) G. Herzberg, *Molecular Spectra and Molecular Structure. I. Spectra of Diatomic Molecules* (van Nostrand, London, 1950); (b) G. Herzberg, II, *Infrared and Raman Spectra of Polyatomic Molecules* (van Nostrand, Princeton, NY, 1945).
[86] J. Ludell, M. Rasanen, and Z. Latajka, Chem. Phys. Lett. **222**, 33 (1994).